



CENTRE DE RECERCA MATEMÀTICA

| | |
|----------------------|--|
| Title: | <i>The melting and solidification of nanowires</i> |
| Journal Information: | <i>Journal of Nanoparticle Research,</i> |
| Author(s): | Florio B.J., Myers T.G.. |
| Volume, pages: | 18 1, DOI:[10.1007/s11051-016-3469-z] |

The melting and solidification of nanowires

B. J. Florio · T. G. Myers

Received: 18 April 2016 / Accepted: 30 May 2016
© Springer Science+Business Media Dordrecht 2016

Abstract A mathematical model is developed to describe the melting of nanowires. The first section of the paper deals with a standard theoretical situation, where the wire melts due to a fixed boundary temperature. This analysis allows us to compare with existing results for the phase change of nanospheres. The equivalent solidification problem is also examined. This shows that solidification is a faster process than melting; this is because the energy transfer occurs primarily through the solid rather than the liquid which is a poorer conductor of heat. This effect competes with the energy required to create new solid surface which acts to slow down the process, but overall conduction dominates. In the second section, we consider a more physically realistic boundary condition, where the phase change occurs due to a heat flux from surrounding material. This removes the singularity in initial melt velocity predicted in previous models of nanoparticle melting. It is shown that even with the highest possible flux the melting time is

significantly slower than with a fixed boundary temperature condition.

Keywords Nanowire · Phase change · Mathematical model · Melting · Modelling and simulation

Introduction

Recent research indicates that in the near future, nanowires will be at the forefront of electronics and computing. It has also been shown that they can be utilised in low cost solar cells, high-power density batteries and flexible screens, to detect proteins to act as cancer biomarkers and for water filtration (Garnett et al. 2011; Liu et al. 2015; Chinen et al. 2015; Ge et al. 2012). In many of these situations, the wires must endure high temperatures or conduct current, which will induce a temperature rise within the wire. With macroscale wires, this may not be an issue since the melt temperature can be high; however, at the nanoscale, it is well-known that material properties can be significantly different from the bulk values, and in particular, the melting point can decrease drastically. The classical study of Buffat and Borel (1976) shows a decrease of approximately 50 % from the bulk value for 1 nm radius gold particles. Molecular dynamics studies have continued to even smaller sizes, with correspondingly larger decreases, while experimental studies on other materials such as tin, lead and

B. J. Florio (✉)
Mathematics Applications Consortium for Science and Industry (MACSI), Department of Mathematics and Statistics, University of Limerick, Limerick, Ireland
e-mail: brendan.florio@ul.ie

T. G. Myers
Centre de Recerca Matemàtica, Campus de Bellaterra,
Edifici C, 08193 Bellaterra, Barcelona, Spain
e-mail: tmyers@crm.cat

drugs also exhibit the same behaviour (Font and Myers 2013). There appears to be less experimental work on the phase change behaviour of nanowires, but it has been shown that they exhibit sintering (a clear indication of melting) well below the bulk melting point (Goswami and Nanda 2010).

In order to use nanowires in practical situations, it is important to understand their behaviour subject to the environmental conditions. For this, we require a theoretical model. There have been a number of studies on the melting behaviour of nanospheres, such as (Font and Myers 2013; Font et al. 2014; McCue et al. 2009; Wu et al. 2009a, b). All of these works use some form of Gibbs–Thomson relation to describe the melting point depression. They also impose a fixed temperature at the outer boundary of the sphere. The results show that initially there is rapid melting (in fact at $t = 0$ the rate is infinite), which subsequently slows down. In the final stages, the melt rate again becomes large as the melt temperature decreases. The final rapid melting predictions have been suggested as an explanation for the experimentally observed sudden disappearance of particles (Kofman et al. 1999). Another common factor in these studies is that they all employ continuum theory. The applicability of continuum theory to phase change models is discussed in detail in Font and Myers (2013); they conclude it is valid down to between 2 and 5 nm depending on the material.

In this paper, we extend the work on nanosphere phase change to nanowires. We will begin with a simple theoretical model, where a cylindrically symmetric wire is melted due to imposing a constant temperature at the outer boundary. The melt temperature will be described by the standard Gibbs–Thomson relation. This initial analysis allows us to clearly demonstrate the solution method and also compare with existing results for nanosphere melting. Next we will consider the converse problem, where solidification proceeds from the boundary. The fixed boundary temperature condition is standard in mathematical studies; however, it is not physically realistic and causes the initial singularity in the melting rate. In the final section, we describe the model where a cooling condition is applied to the outer boundary. This is more physically realistic and removes the initial singularity. In all cases, the calculations will be terminated when the radius is around 2 nm, to ensure the results do not pass beyond the continuum limit.

Nanowire melting

In this initial work, we will make a number of assumptions which are standard in the theoretical literature:

1. The wire is cylindrically symmetric and remains in this state throughout the melting process;
2. The density is the same in the solid and liquid phases;
3. Melting occurs due to the boundary being heated instantaneously to a constant temperature greater than the melt temperature; and
4. Surface tension and latent heat are constant.

Later on we will discuss relaxing certain of these assumptions. When required we will take parameter values for gold, since this is a common material for experiments at the nanoscale, and there is also a large amount of experimental data concerning gold's properties. The parameter values we use for gold are given in Table 1.

Consider a nanowire of radius R_0 , initially at some temperature which is below the melt temperature T_m . At time $t = 0$, the boundary is heated to a temperature $T_H > T_m$, so initiating the melt process (note, in the “Newton cooling at the outer boundary” section, we will provide analysis for a physically realistic boundary condition). As the melting proceeds, the position of the melt interface is denoted by $r = R(t)$; melting is complete when $R(t) = 0$. A schematic of the system is provided in Fig. 1. The axisymmetric heat equations in cylindrical coordinates are given by

Table 1 Thermophysical parameter values for gold

| | Value | Units |
|---------------|--------------------|----------------------------------|
| k_s | 317 | $\text{W m}^{-1} \text{K}^{-1}$ |
| k_l | 106 | $\text{W m}^{-1} \text{K}^{-1}$ |
| L | 6.37×10^4 | J kg^{-1} |
| c_s | 129 | $\text{J kg}^{-1} \text{K}^{-1}$ |
| c_l | 163 | $\text{J kg}^{-1} \text{K}^{-1}$ |
| ρ_s | 1.93×10^4 | kg m^{-3} |
| T_m^* | 1337 | K |
| σ_{sl} | 0.27 | N m^{-1} |

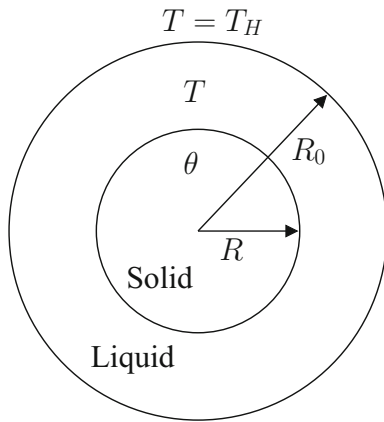


Fig. 1 A schematic of the melting nanoparticle. The solid is initially of size $r = R_0$, the solid–liquid interface is located at $r = R(t)$

$$c_l \rho_l \frac{\partial T}{\partial t} = \frac{k_l}{r} \frac{\partial}{\partial r} \left(r \frac{\partial T}{\partial r} \right) \text{ for } R < r < R_0, \quad (1)$$

$$c_s \rho_s \frac{\partial \theta}{\partial t} = \frac{k_s}{r} \frac{\partial}{\partial r} \left(r \frac{\partial \theta}{\partial r} \right) \text{ for } 0 < r < R, \quad (2)$$

for the liquid and solid phases, respectively. Here ρ denotes the density, c the specific heat, k the thermal conductivity, subscripts l and s denote the liquid and solid properties, respectively. To simplify the model, from henceforth we will use a value $\rho_s = \rho_l$. Appropriate boundary conditions are

$$T(R_0, t) = T_H, \quad \left. \frac{\partial \theta}{\partial r} \right|_{r=0} = 0, \quad (3)$$

$$T(R, t) = \theta(R, t) = T_m(t).$$

These denote a fixed temperature boundary, symmetry at the origin and that the solid and liquid temperatures are at the melt temperature $T_m(t)$ at $r = R(t)$. The melt temperature variation may be approximated by the Gibbs–Thomson equation

$$T_m(t) = T_m^* \left(1 - \frac{2\sigma_{sl}}{\rho_s L_m} \kappa(t) \right), \quad (4)$$

where T_m^* is the bulk melting temperature, σ_{sl} is the solid–liquid surface tension, L_m is the latent heat of fusion and κ is the mean curvature. For a cylindrically symmetric geometry with inwards melting, the mean curvature is $\kappa = 1/(2R(t))$. Both surface tension and

latent heat have also been observed to decrease with decreasing radius; however, for simplicity and to conform with previous studies, we will take these to be constant.

We impose a single initial condition $R(0) = R_0$. The initial conditions for the temperature can be problematic since the liquid phase does not exist at $t = 0$. However, neglecting to specify the temperatures at $t = 0$ does not cause any problems since the solution technique employed in the following section does not require initial temperature values.

To determine the position of the interface a Stefan condition is imposed. This is a statement of energy balance

$$(\rho_s L_m - 2\sigma_{sl} \kappa) \frac{dR}{dt} = k_s \frac{\partial \theta}{\partial r} - k_l \frac{\partial T}{\partial r}, \quad (5)$$

where all quantities are evaluated at $r = R$. The standard Stefan condition states that the latent heat release is balanced by the energy conducted through the two phases. The above equation includes a modification appropriate at the nanoscale. Energy is required to create new surfaces, or released when surfaces shrink; consequently, a surface energy term is added to our energy balance (Hennessy 2010; Davis 2001). This is true for surfaces of any size; however, at the nanoscale, the surface energy is usually negligible. For gold, $\rho_s L_m \approx 1.1 \times 10^9 \text{ J/m}^3$, while $\sigma_{sl}/R \approx 0.27/R \text{ J/m}^3$, consequently the surface energy term only plays a significant role for radii of the order of nanometres. Note, Eq. (5) is significantly different to that employed in the theoretical studies mentioned in the introduction. In those works, the surface energy term is replaced by $(c_l - c_s)(T_m - T_m^*)$. This term occurs due to an assumption that latent heat is released at the bulk melt temperature. Obviously this is incorrect (see the experimental results in Liu and Wang (2013), for example); so we prefer the corrected form derived in Myers (2016) which involves latent heat release at the actual phase change temperature.

As the solid–liquid interface proceeds inwards due to melting, latent heat is absorbed and is usually taken in the form of thermal energy. Simultaneously, the surface releases energy as it shrinks, offsetting the thermal energy required to advance the melting front. Thus, we expect the surface energy term to accelerate the melting process.

Non-dimensional model

We now introduce the dimensionless variables

$$\hat{T} = \frac{T - T_m^*}{\Delta T}, \quad \hat{\theta} = \frac{\theta - T_m^*}{\Delta T}, \quad \hat{r} = \frac{r}{R_0},$$

$$\hat{R} = \frac{R}{R_0}, \quad \hat{t} = \frac{k_1}{\rho_s c_1 R_0^2} t, \quad \hat{T}_m = \frac{T_m - T_m^*}{\Delta T}. \quad (6)$$

The temperature scale is defined as the difference between the boundary and bulk melt temperature, $\Delta T = T_H - T_m^* > 0$. The time scale is that for heat to diffuse through the liquid layer. Dropping the hat notation, the dimensionless heat equations are

$$\frac{\partial T}{\partial t} = \frac{1}{r} \frac{\partial}{\partial r} \left(r \frac{\partial T}{\partial r} \right), \text{ for } R < r < 1, \quad (7)$$

$$\frac{\partial \theta}{\partial t} = \frac{k}{c} \frac{1}{r} \frac{\partial}{\partial r} \left(r \frac{\partial \theta}{\partial r} \right), \text{ for } 0 < r < R, \quad (8)$$

where $k = k_s/k_l$ and $c = c_s/c_l$. The boundary conditions are

$$T(1, t) = 1 \quad \left. \frac{\partial \theta}{\partial r} \right|_{r=0} = 0 \quad T(R, t) = \theta(R, t) = T_m.$$

The dimensionless Gibbs–Thomson relation is

$$T_m = -\frac{\Gamma}{2R}, \quad (9)$$

where $\Gamma = 2\sigma_{sl}T_m^*/(\rho_s L_m R_0 \Delta T)$. From (5), the dimensionless Stefan condition is given by

$$\left(\beta - \frac{\Lambda}{2R} \right) \frac{dR}{dt} = k \frac{\partial \theta}{\partial r} - \frac{\partial T}{\partial r}, \quad (10)$$

where the Stefan number is defined as $\beta = L_m/c_l \Delta T$, and $\Lambda = 2\sigma_{sl}/(c_l \Delta T \rho_s R_0)$. The initial radius is $R(0) = 1$.

Only a small amount of energy is required to melt a nanoparticle; once melting begins the decrease in melt temperature means that the process tends to proceed rapidly. For this reason, only a small ΔT is required to completely melt the particle. Consequently, nanoparticle melting typically involves a large Stefan number (Font and Myers 2013; Font et al. 2014). For gold, with $\Delta T = 10$, we find $\beta \approx 40$. A large Stefan number indicates melting occurs on a much longer time scale to heat diffusion so, to analyse the melting process, it is better to work on the melting time scale. This requires

rescaling time so that $t = \beta \tau$, so when t is of order β the time variable τ is order unity. The heat equations and Stefan condition now become

$$\frac{1}{\beta} \frac{\partial T}{\partial \tau} = \frac{1}{r} \frac{\partial}{\partial r} \left(r \frac{\partial T}{\partial r} \right) \quad \frac{1}{\beta} \frac{\partial \theta}{\partial \tau} = \frac{k}{c} \frac{1}{r} \frac{\partial}{\partial r} \left(r \frac{\partial \theta}{\partial r} \right), \quad (11)$$

$$\left(1 - \frac{1}{\beta} \frac{\Lambda}{2R} \right) \frac{dR}{d\tau} = k \frac{\partial \theta}{\partial r} - \frac{\partial T}{\partial r}. \quad (12)$$

From Table 2, it is clear that Λ is order unity (or smaller) and so the term involving Λ/β will not appear in the leading order balance.

Solution method

We now carry out a standard perturbation analysis based on the small parameter $1/\beta$. The accuracy of this approach has been demonstrated in studies on nanosphere phase change by comparison with the numerical solution of the full problem (Font and Myers 2013; Font et al. 2014). The temperatures are expressed in terms of series

$$T = T_0 + \frac{1}{\beta} T_1 + \mathcal{O}\left(\frac{1}{\beta^2}\right), \quad \theta = \theta_0 + \frac{1}{\beta} \theta_1 + \mathcal{O}\left(\frac{1}{\beta^2}\right). \quad (13)$$

Substituting these into the heat equations and collecting terms at the same order of $1/\beta$ gives the leading order equations

$$0 = \frac{1}{r} \frac{\partial}{\partial r} \left(r \frac{\partial T_0}{\partial r} \right) \quad 0 = \frac{k}{c} \frac{1}{r} \frac{\partial}{\partial r} \left(r \frac{\partial \theta_0}{\partial r} \right). \quad (14)$$

The lack of time derivative in these equations indicates that the heat flow is so fast compared to the melting that the temperature approximately reaches a steady state (within order $1/\beta$) for each particle size. This is also why we do not need initial conditions for the temperature: the heat evolution is approximately

Table 2 Dimensionless parameter values for relevant R_0 and β

| | | | |
|---------------|-----------|-------|--------|
| $\beta = 100$ | R_0 | 10 nm | 100 nm |
| | Γ | 15.0 | 1.50 |
| | Λ | 4.39 | 0.439 |
| $\beta = 10$ | R_0 | 10 nm | 100 nm |
| | Γ | 1.50 | 0.150 |
| | Λ | 0.439 | 0.0439 |

independent of the initial value. The reduction is not truly steady state since the boundary conditions involve the time-dependent radius, $R(t)$. Consequently this is termed a quasi—or pseudo-steady reduction. The leading order equations must be solved subject to

$$\begin{aligned} T_0(1, \tau) = 1 \quad \frac{\partial \theta_0}{\partial r} \Big|_{r=0} &= 0, \\ \theta_0(R, \tau) = T_0(R, \tau) = T_m. \end{aligned} \quad (15)$$

This leads to

$$T_0 = (T_m - 1) \frac{\ln(r)}{\ln(R)} + 1 \quad \theta_0 = T_m. \quad (16)$$

These solutions show that the temperature in the solid, θ , is approximately independent of distance and depends only on the value of the melt temperature. The liquid temperature decreases logarithmically from the boundary value $T = 1$ to the melt temperature at the interface. These two expressions provide a first approximation to the temperature and may be used in the Stefan condition to determine the position R . However, we may improve accuracy by looking for a correction due to the next order terms.

At $\mathcal{O}(1/\beta)$:

$$\frac{\partial T_0}{\partial \tau} = \frac{1}{r} \frac{\partial}{\partial r} \left(r \frac{\partial T_1}{\partial r} \right) \quad \frac{\partial \theta_0}{\partial \tau} = \frac{k}{c} \frac{1}{r} \frac{\partial}{\partial r} \left(r \frac{\partial \theta_1}{\partial r} \right), \quad (17)$$

subject to

$$\begin{aligned} T_1(1, \tau) = 0 \quad \frac{\partial \theta_1}{\partial r} \Big|_{r=0} &= 0, \\ \theta_1(R, \tau) = T_1(R, \tau) = 0. \end{aligned} \quad (18)$$

This has solution

$$\begin{aligned} T_1 &= \frac{R_\tau}{8} \left(\frac{\Gamma \ln(R) + \Gamma + 2R}{R^2 \ln(R)^2} \right) \\ &\quad \times \left((r^2 \ln(r) - r^2 + 1) - (R^2 \ln(R) - R^2 + 1) \frac{\ln(r)}{\ln(R)} \right), \\ \theta_1 &= \frac{c\Gamma}{8kR^2} R_\tau (r^2 - R^2). \end{aligned} \quad (19)$$

Taking the leading and first-order terms for T, θ and substituting into the Stefan condition, Eq. (11), we obtain an equation for the evolution of the radius

$$R_\tau = \frac{dR}{d\tau} = \frac{2R + \Gamma}{2R^2 \ln(R) \left(1 + \frac{1}{\beta} \left(\mu - \frac{\Lambda}{2R} - \frac{c\Gamma}{4R} \right) \right)}, \quad (20)$$

where

$$\mu = \left(\frac{2R + \Gamma(1 + \ln(R))}{8R^3 \ln(R)^3} \right), \quad (21)$$

$$\times \left(R^2 - 1 + 2R^2 \ln(R) (\ln(R) - 1) \right). \quad (22)$$

Note, from the above equations, it is clear that the model predicts two singularities, where the velocity becomes infinite. These are when $R = 1$ (so $\ln(R) = 0$) and $R = 0$. The first of these is a consequence of the fixed temperature boundary condition. At $t = 0$ the boundary is instantaneously heated to a value $T_H > T_m^*$. This results in an infinite temperature gradient at the boundary and consequently an infinite boundary velocity. This is unphysical and will be discussed in further detail in the “[Newton cooling at the outer boundary](#)” section. The second singularity, as $R \rightarrow 0$ is a run-away effect resulting from applying a finite boundary temperature to a particle whose size is tending to zero, this is aided by the rapidly decreasing melt temperature. However, since we require radii of greater than 2 nm, this singularity is never achieved.

Results

The problem has now been reduced from solving two partial differential equations coupled to an ordinary differential equation which defines the domain to solving a single, first-order ordinary differential equation. The numerical solution of Eq. (20), subject to $R(0) = 1$ is a trivial task: we employed the numerical solver in *Mathematica*. Once R is known the temperature profiles may be calculated from Eqs. (16, 19). In Fig. 2, we present results showing the evolution of R for two initial radii, $R_0 = 10, 100$ nm and two values of the Stefan number $\beta = 10, 100$. All other parameter values are taken from Table 1. The lower Stefan number corresponds to a hotter surface and so results in faster melting. The dimensional melting times of the nanowire for Fig. 2a, b, c and d are given by $t = 2520, 623, 3.56$ and 2.52 ps, respectively. The solid line on figure shows the results of the current study for a melting nanowire; for comparison purposes, we also show the equivalent curve (dotted line)

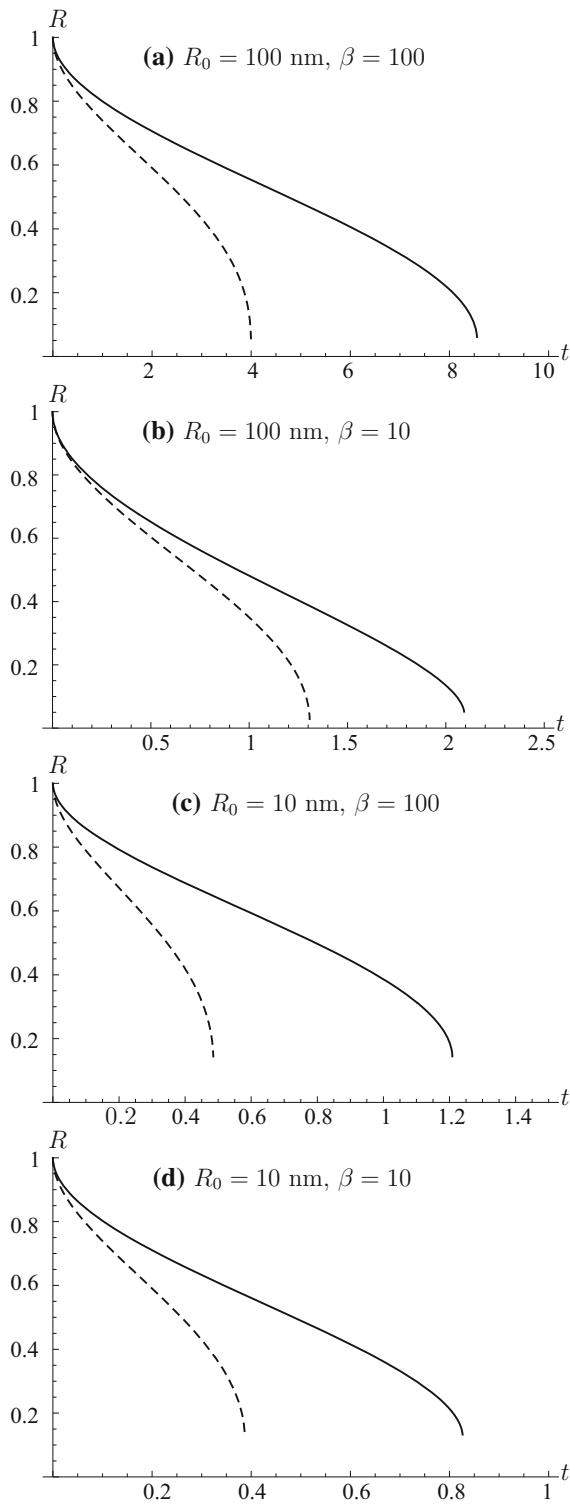


Fig. 2 The dimensionless location of the solid–liquid interface R as a function of time for different values of R_0 and β , for a gold nanowire (solid) and nanosphere (Font and Myers 2013) (dashed)

for the melting of a nanosphere, see Font and Myers (2013). In all cases, we stop the calculation around 2 nm, where we expect continuum theory to break down. Qualitatively, the two sets of curves are the same, with initial and final rapid melting; however, the sphere melts much faster than the wire. This should be expected since the sphere has a greater surface to volume ratio than the wire, thus allowing more rapid heat absorption. As the mean curvature of a sphere is greater than the curvature of a wire of the same radius, the melting point depression is much more severe in a sphere, further speeding the melting process.

Figure 3 shows an example of how the temperature profile changes in time. The dashed line represents the non-dimensional melt temperature, specified by the Gibbs–Thomson relation. This demonstrates how the melt temperature rapidly decreases with size. Curves on the right represent the liquid temperature, which decrease from $T = 1$ at $R = 1$ to T_m at $r = R$. To the left of the intersection with T_m , they are the curves for the solid temperature. The curves clearly have a similar form to those presented in Font and Myers (2013) and Font et al. (2014) for nanosphere melting. As the melting front proceeds inwards, the phase

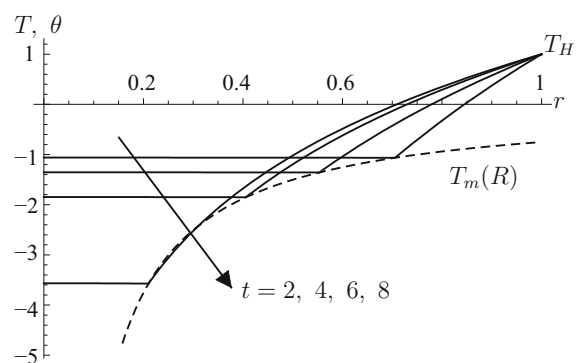


Fig. 3 The dimensionless temperature profile at different times for $R_0 = 100$ nm and $\beta = 100$. The dashed line represents the melt temperature specified by the Gibbs–Thomson Eq. (9)

change temperature is depressed further and the temperature difference, $T_H - T_m$, increases. Thus, we have a run-away result where it becomes easier to melt the wire as melting proceeds.

Solidification of a cylindrical liquid

We now consider the converse problem to that described above, namely, the solidification of a cylindrical liquid sample. Physically, this situation could occur if a nanowire were partially melted due to a high current which has been switched off before the melt process has been completed. In keeping with the previous section, re-solidification occurs due to the outer boundary being maintained below the phase change temperature.

The analysis of this section follows closely with that of the previous section, with two important sign changes. First, the curvature is now $\kappa = -1/(2R)$. The temperature scale $\Delta T = T_H - T_m$ used in the non-dimensionalisation (6) is negative and must be replaced with $|\Delta T|$. The phase change temperature now increases with decreasing particle size. This superheating of the phase change temperature in embedded metallic particles is consistent with experimental observations (Xiong et al. 2011). The negative curvature also affects the Stefan condition; now as the solid-liquid interface moves inwards, latent heat is released as thermal energy rather than absorbed. The surface physics remain the same; as the interface shrinks it releases energy. In the previous case, these were competing effects and resulted in speeding up the melting as the solid size decreased, now they combine and act to slow down the solidification process. However, as we will see, this effect is small compared to the effect of conduction.

The non-dimensional problem is now described by (7) for $0 < r < R$ and (8) for $R < r < 1$. The Gibbs–Thomson relation becomes

$$T_m = \frac{\Gamma}{2R}, \quad (23)$$

where $\Gamma = 2\sigma_{sl}T_m^*/(\rho_s L_m R_0 |\Delta T|)$. The Stefan condition is

$$\left(\beta + \frac{\Lambda}{2R}\right) \frac{dR}{dt} = k \frac{\partial \theta}{\partial r} - \frac{\partial T}{\partial r}, \quad (24)$$

where $\beta = L_m/(c_l |\Delta T|)$ and $\Lambda = 2\sigma_{sl}/(R_0 c_l \rho_s |\Delta T|)$. Since the solid now occupies the outer region and the inner is liquid, we change two boundary conditions

$$\theta(1, t) = -1 \quad \left. \frac{\partial T}{\partial r} \right|_{r=0} = 0. \quad (25)$$

As in the previous section, we rescale time $t = \beta\tau$ and use a perturbation method. At leading order, we obtain

$$\theta_0 = (T_m + 1) \frac{\ln(r)}{\ln(R)} - 1 \quad T_0 = T_m. \quad (26)$$

At first order, $\mathcal{O}(1/\beta)$, the temperatures are

$$\begin{aligned} \theta_1 &= \frac{-cR_\tau}{k} \frac{8}{\ln(R)^2} \left(\frac{\Gamma \ln(R) + \Gamma + 2R}{R^2 \ln(R)^2} \right) \\ &\quad \times \left((r^2 \ln(r) - r^2 + 1) - (R^2 \ln(R) - R^2 + 1) \frac{\ln(r)}{\ln(R)} \right), \\ T_1 &= \frac{-\Gamma}{8R^2} R_\tau (r^2 - R^2). \end{aligned} \quad (27)$$

Now we substitute for T, θ into the Stefan condition to obtain

$$R_\tau = \frac{dR}{d\tau} = \frac{k(2R + \Gamma)}{2R^2 \ln(R) \left(1 + \frac{1}{\beta} \left(c\mu + \frac{\Lambda}{2R} - \frac{\Gamma}{4R} \right) \right)}, \quad (28)$$

where μ is defined in (21). Comparison with Eq. (20) shows a key difference in the two processes. Equation (28) contains a factor k (the ratio of solid to liquid conductivities) on the right-hand side. Since the solid phase is a better conductor than the liquid phase $k > 1$, we must expect the solidification process to be faster than the corresponding melting process. The first-order correction terms (the $1/\beta$ terms in the denominator) show that the ratio of specific heats, c and surface energy, Λ , also play a role. However, it is the fact that energy is now conducted through the solid that makes the greatest difference between the melting and solidification processes.

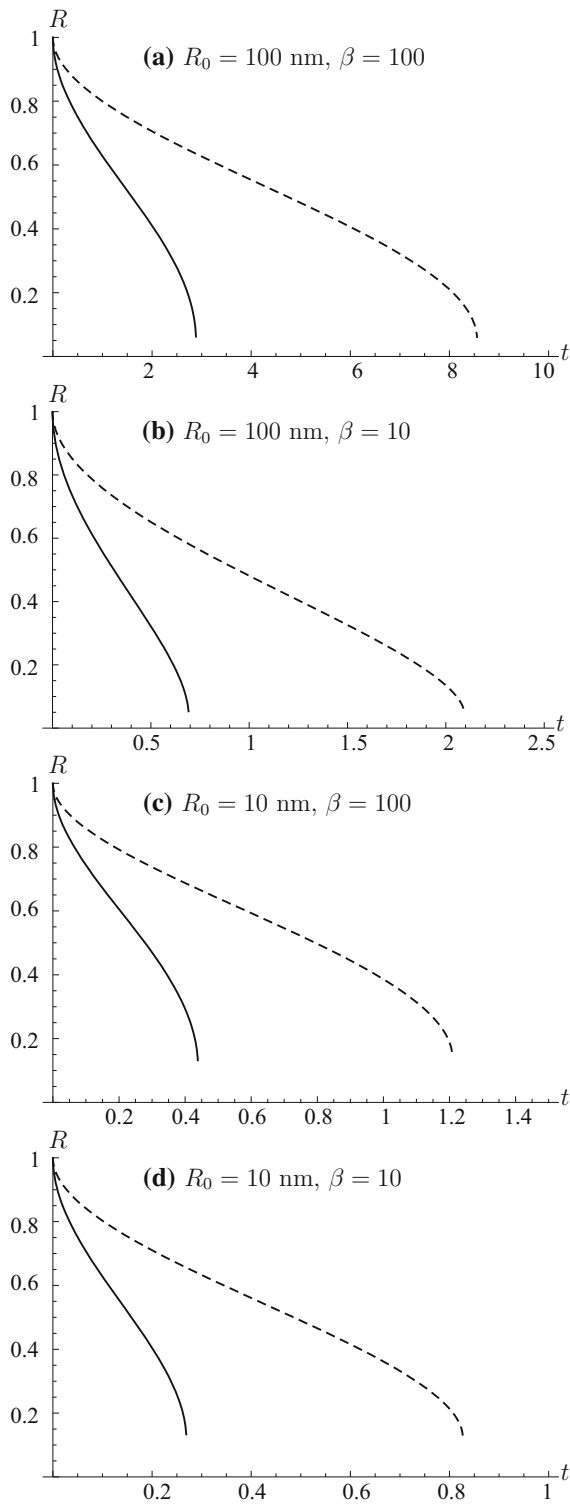


Fig. 4 The dimensionless location of the solid–liquid interface R as a function of time for different values of R_0 and β , for a solidifying gold nanowire (*solid*) and the melting nanowire from the “Nanowire melting” section (*dashed*)

Results

We now compare the solidification and melting process using the same numerical procedure as in the “Nanowire melting” section. The evolution of the solid–liquid interface for the melting and solidification problem for $R_0 = 10, 100$ nm and $\beta = 10, 100$ are shown in Fig. 4 (again cut-off at around 2 nm). Qualitatively, the two profiles are very similar. The ratio $k = k_s/k_l \approx 3$ and, as discussed above, this

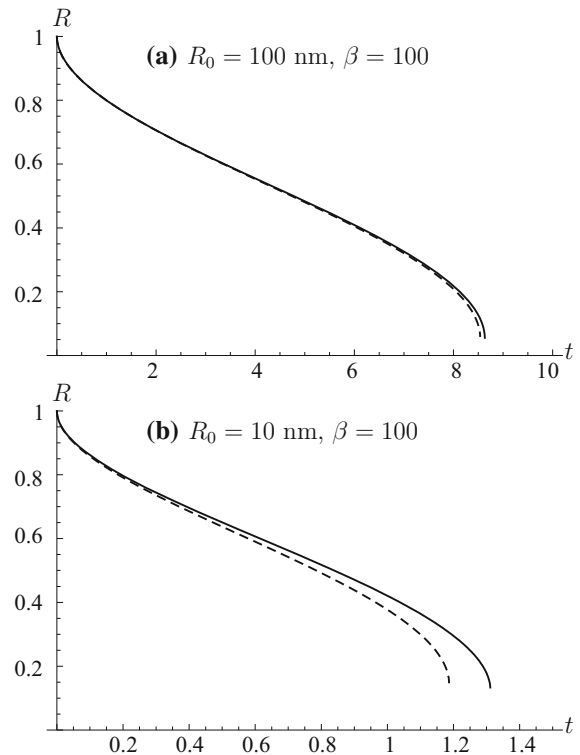


Fig. 5 The dimensionless location of the solid–liquid interface R as a function of time for $\beta = 100$ and different values of R_0 , for a solidifying gold nanowire (*solid*) and the melting nanowire from the “Nanowire melting” section (*dashed*) for $c = k = 1$. The surface energy term becomes important for small values of R , which is why the difference is prominent in (b) for $R_0 = 10$ nm

translates to solidification roughly three times as fast as melting. The dimensional solidification times corresponding to the solid lines in Fig. 4a, b, c and d are given by $t = 890, 208, 1.33$ and 0.742 ps, respectively (this may be compared with the corresponding times for melting of 2520, 623, 3.56 and 2.52 ps, respectively).

To demonstrate the effect of the surface energy, in Fig. 5 we compare the melting and solidification process for a situation where $k = c = 1$. Now the difference in the models is purely due to the effect of the shrinking interface which releases (rather than absorbs) energy. This acts to slow down the process. As can be seen in figures, when $R_0 = 100$ nm, the difference between the melting and solidifying wires is negligible. Only in the very final moments is any difference visible. This can be traced to the fact that $\Lambda \propto 1/R_0$ is small for a large particle. In the second figure, where $R_0 = 10$ nm, surface energy plays a more important role and the difference is much greater. Now the solidification process takes noticeably longer than melting, confirming the statement that the energy release slows down the process. However, in the general case, where $k \neq 1$, it is the conduction effect which dominates and solidification occurs at a much faster rate than melting.

In Fig. 6, the temperature profiles in the solid and liquid phases are shown for $R_0 = 100$ nm, $\beta = 100$. Obviously this resembles an inverted version of Fig. 3. Again we see that the phase change is a run-away process. As the liquid region decreases in size, the solidification temperature increases. Since the edge of the solid is maintained at a constant temperature $T_H < T_m$ the higher the value of T_m the larger the

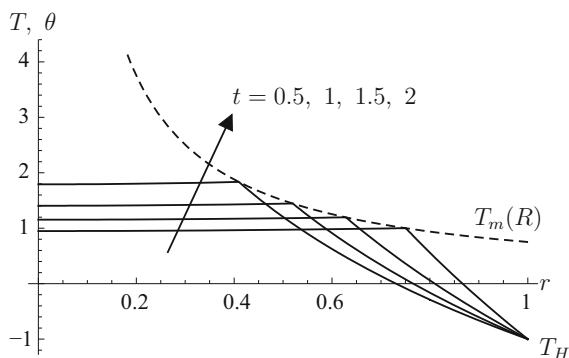


Fig. 6 The dimensionless temperature profile at different times for $R_0 = 100$ nm and $\beta = 100$. The dashed line represents the melt temperature specified by the Gibbs–Thomson Eq. (23)

temperature difference and the more rapid the solidification.

Newton cooling at the outer boundary

As discussed in the introduction, the fixed temperature boundary condition is not physically realistic and is generally applied for mathematical convenience. As a result of the unphysical nature of the formulation, the mathematical solution encounters difficulties. To understand the issues consider a material that is initially at a temperature T_i , and then at the boundary, the temperature is instantaneously changed to a different value. Since the distance between the boundary and the material touching the boundary is infinitely small (to mathematicians at least), the corresponding temperature gradient (and hence energy flux), $\Delta T/\Delta x$, is infinite. With Stefan problems, the rate at which the phase change front moves is proportional to the difference in temperature gradients. The initial infinite temperature gradient resulting from the instantaneous temperature change then leads to an infinite initial melt rate. In the results of the previous section, we can see this infinite rate through the gradient of R at $t = 0$: Eqs. (20, 28) show $R_t \propto 1/\ln(R)$, where initially $\ln(R(0)) = \ln(1) = 0$.

In reality, a finite amount of energy is input at the boundary, in such a way that the phase change proceeds in a smooth fashion. This may be expressed through boundary conditions such as the cooling condition or a prescribed energy flux. For the melting problem, in dimensional form, these are

$$-k_l \frac{\partial T}{\partial r} = h(T - T_H) \quad , \quad -k_l \frac{\partial T}{\partial r} = q, \quad (29)$$

where h is the heat transfer coefficient and q the flux. Note, if $T_H > T$ then this condition implies heating at the boundary. We will now analyse melting subject to the first of these conditions since it is the more general and both prescribed flux and fixed temperature conditions may be seen as limiting cases of the cooling condition. Specifically the fixed temperature condition of the previous section corresponds to an infinite heat transfer coefficient. To allow comparison between the cooling condition and fixed temperature models, we will thus assume a large value for h . However, there are physical limits to the heat transfer, too much energy would simply vaporise the material, and so we will use a maximum value defined by

$$h_{\max} = \frac{q_{\max}}{\Delta T}, \quad q_{\max} = \rho_s u v_s, \quad (30)$$

where u is the internal energy and v_s is the speed of second sound in the material, see Jou et al. (2010). The maximum flux is a requirement for thermodynamic stability. We may estimate a typical order of magnitude for h_{\max} by first noting that the speed of second sound may be related to the phonon velocity $v_s = v_p/\sqrt{3}$. We follow Zhang et al. (2011) and take $v_p = \sqrt{B/\rho_s} \approx 3000 \text{ m/s}$ (B is the bulk modulus). The internal energy is given approximately by the enthalpy (this is valid under constant pressure, constant density and zero velocity), $u = c_s \Delta T$, consequently in the following results we will employ a maximum value $h_{\max} = \rho_s c_s v_s \approx 4.4 \times 10^9 \text{ W/m}^2 \text{ K}$.

In non-dimensional form, the cooling condition, which is applied at $r = 1$, is

$$\frac{\partial T}{\partial r} = -\text{Nu}(T - 1), \quad (31)$$

where Nu is the Nusselt number given by $\text{Nu} = hR_0/k_l$. Following the perturbation method described in the “Solution method” section, we have at leading order

$$\frac{\partial T_0}{\partial r} = -\text{Nu}(T_0 - 1), \quad (32)$$

which leads to

$$T_0 = \left(\frac{\text{Nu} \ln(r) - 1}{\text{Nu} \ln(R) - 1} \right) (T_m - 1) + 1, \quad \theta_0 = T_m. \quad (33)$$

At $\mathcal{O}(1/\beta)$, the cooling condition reduces to

$$\frac{\partial T_1}{\partial r} = -\text{Nu} T_1. \quad (34)$$

With corresponding solution,

$$\begin{aligned} T_1 &= R_\tau \left(\frac{(\text{Nu} \ln(R) - 1) \frac{\partial T_m}{\partial R} - \frac{\text{Nu}(T_m - 1)}{R}}{(\text{Nu} \ln(R) - 1)^2} \right) \\ &\quad \times \left(A \ln(r) + B + \frac{1}{4} r^2 (\text{Nu} (\ln(r) - 1) - 1) \right), \\ \theta_1 &= \frac{c\Gamma}{8kR^2} R_\tau (r^2 - R^2). \end{aligned} \quad (35)$$

where

$$A = \frac{\text{Nu} R^2 (\text{Nu} (-\ln(R)) + \text{Nu} + 1) - \text{Nu} (\text{Nu} + 2) - 2}{4\text{Nu} \ln(R) - 4}, \quad (36)$$

$$B = \frac{R^2 (\text{Nu} \ln(R) - \text{Nu} - 1) + (\text{Nu} (\text{Nu} + 2) + 2) \ln(R)}{4\text{Nu} \ln(R) - 4}. \quad (37)$$

For the case of melting a cylindrical wire, the Stefan condition (11) holds. With a cooling condition, the expression for the Stefan condition to first order in $1/\beta$ is rather cumbersome so we will now only write down the leading order form

$$\frac{\partial R}{\partial \tau} = -\frac{\text{Nu}(T_m - 1)}{R(\text{Nu} \ln(R) - 1)} = \frac{\text{Nu}(2R + \Gamma)}{2R^2(\text{Nu} \ln(R) - 1)}. \quad (38)$$

In the limit $\text{Nu} \rightarrow \infty$, we find $R_\tau \rightarrow (2R + \Gamma)/(2R^2 \ln R)$, which coincides with the leading order terms of equation (20). That is, in the limit of infinite heat transfer coefficient, we retrieve the solution from

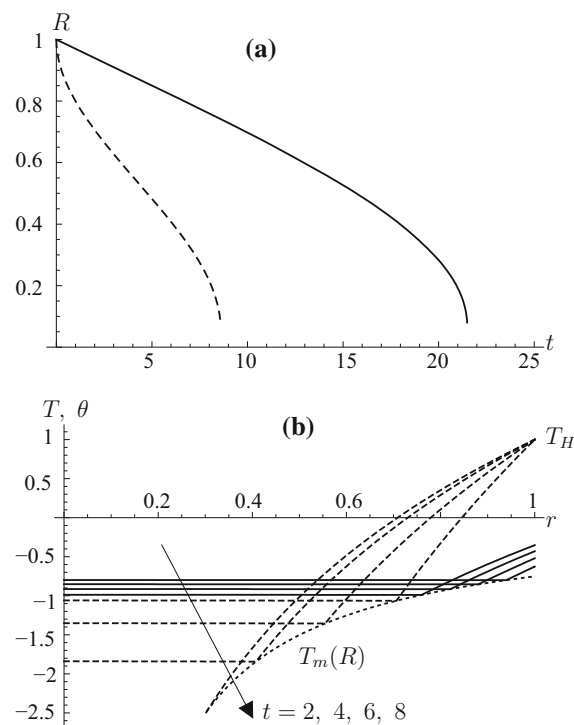


Fig. 7 **a** The time evolution of the solid–liquid interface (solid line is the cooling condition model, dashed line the fixed boundary temperature) and **b** the temperature profile at various times, both for $R_0 = 100 \text{ nm}$, $\beta = 100$

the fixed boundary temperature problem. However, obviously $Nu \neq \infty$, in which case it is clear from the above formula that the singularity at $R(0) = 1$ has been removed. The second singularity, at $R = 0$ (which is never reached), still remains.

The evolution of the solid–liquid interface and the temperature profiles at different times can be seen in Fig. 7. We use the maximum value of the Nusselt number, i.e. $Nu = h_{\max}R_0/k_l \approx 1.72$ for a 100 nm radius wire and $\beta = 100$. This should give us the closest results to those of the fixed temperature boundary condition. Comparison of the two curves in Fig. 7a shows that even for the maximum heat transfer, the solutions are quite different. First, as discussed already, the initial singularity in velocity no longer occurs. The gradient is finite and can be calculated from (38), $R_\tau = -Nu(2 + \Gamma)/2$. In fact, the gradient is approximately constant for most of the process, only increasing in magnitude near the end, resulting in a final melt time close to $t = 21.5$ (or dimensionally, $t = 6.38$ ns). The corresponding result for a fixed temperature boundary condition, shown in Fig. 2a, predicts complete melting for $t \approx 9.5$, more than twice as fast as with a cooling condition. This can be related to the fact that the fixed temperature condition corresponds to an infinite heat transfer coefficient and so the exterior heat is immediately transmitted to the particle. With a cooling condition, not all the energy is transmitted, resulting in a slower process. A series of temperature profiles are shown in Fig. 7b. The forms are similar to that of Fig. 3, but the boundary temperature is lower than in the fixed temperature problem. This results in a lower temperature gradient and hence slower melting.

Conclusion

A mathematical model has been developed to describe the melting of nanowires. In the first section, we imposed a fixed temperature at the outer boundary and considered melting or solidification due to this temperature. This allowed us to follow on from previous analytical work and to compare with results for nanospheres. Noting that the fixed temperature condition is primarily imposed for mathematical convenience in the second section, we considered a more physically realistic condition, where the energy input at the boundary is due to a surrounding material at a

different temperature. All of the analysis was based on continuum theory which, as discussed in the introduction, should not be trusted for particle radii smaller than 2 nm. The physical situation was treated in an idealistic way, ignoring impurities or instabilities, so the results could also be viewed as the base case for more complex analyses.

Comparing equivalent results for the melting of nanowires and nanospheres with a fixed boundary condition, showed that spherical particles melt typically three times as fast as wires of the same radius. This could be attributed to two factors. First, heat can enter the sphere more efficiently: the ratio of surface to volume is $3/R$ for the sphere and $2/R$ for the wire, so there is proportionally more surface for the heat to enter. Second, the Gibbs–Thomson relation predicts a more rapid decrease in melt temperature for the sphere. This is because the temperature decrease is related to the mean curvature, which is greater for a sphere ($\kappa = 1/R$ as opposed to $1/(2R)$).

The analysis on the solidification of a cylindrical liquid sample contained within a solid clearly demonstrated that solidification occurs at a faster rate than melting under equivalent conditions. This could be attributed to the heat transfer from the boundary through the solid phase, since the solid phase will conduct heat better than the liquid. There was a competing effect, namely, the creation of new solid surface, which requires energy. However, the contribution from this was significantly less than the effect of the increased heat transfer.

Results for both melting and solidification showed singularities in the melt rate at the start and end of the process. This has been observed in previous theoretical studies on nanosphere melting. The singularity predicted by the mathematical model at the end of the process has been used to explain the experimentally observed rapid disappearance of small particles (Kofman et al. 1999; McCue et al. 2009; Wu et al. 2009a). However, it is worth pointing out that since continuum theory breaks down before the radius reaches zero, the model prediction is merely an indication of how the particle disappears. A more rigorous analysis of the final stages of melting would require linking the present model to a discrete one (although given the qualitative similarities between experiment and theory a more detailed analysis seems unlikely to have any significant effect on the melt times predicted by the current model). Noting that the fixed temperature

condition is physically unrealistic, in the final section of the paper, we applied a Newton cooling condition at the outer boundary. This showed that the initial singularity was a product of imposing an unrealistic condition: the cooling condition showed no such singularity. Even with the highest possible imposed heat flux, the cooling condition shows significantly slower melt times than those predicted with a fixed temperature condition. This conclusion will also hold for all previous theoretical studies on nanosphere melting.

Acknowledgments The research of BF is supported by MACSI funded by the Science Foundation Ireland Grant 12/IA/1683, Royal Irish academy Charlemont Grant 2015 and a MI-NET cost short-term scientific mission, COST-STSM-TD1409-30100. TM acknowledges financial support from the Ministerio de Ciencia e Innovación Grant MTM 2014-56218.

References

- Buffat P, Borel JP (1976) Size effect on the melting temperature of gold particles. *Phys Rev A* 13:2287–2297
- Chinen AB, Guan CM, Ferrer JR, Barnaby SN, Merkel TJ, Mirkin CA (2015) Nanoparticle probes for the detection of cancer biomarkers, cells, and tissues by fluorescence. *Chem Rev* 115:10530–10574
- Davis SH (2001) *Theory of solidification*. Cambridge University Press, Cambridge
- Font F, Myers TG (2013) Spherically symmetric nanoparticle melting with a variable phase change temperature. *J Nanopart Res* 15:2086
- Font F, Myers TG, Mitchell SL (2014) A mathematical model for nanoparticle melting with density change. *Microfluid Nanofluid* 18:233–243
- Garnett EC, Brongersma ML, Cui Y, McGehee MD (2011) Nanowire solar cells. *Ann Rev Mater Res* 41(1):269–295
- Ge M, Rong J, Fang X, Zhou C (2012) Porous doped silicon nanowires for lithium ion battery anode with long cycle life. *Nano Lett* 12:2318–2323
- Goswami GK, Nanda KK (2010) Size-dependent melting of finite-length nanowires. *J Phys Chem* 114:14327–14331
- Hennessy MG (2010) Liquid snowflake formation in superheated ice. Master's Thesis, University of Oxford, Oxford
- Jou D, Casas-Vázquez J, Lebon G (2010) *Extended irreversible thermodynamics*, 4th edn. Springer, Berlin
- Kofman R, Cheyssac P, Lereah Y, Stella A (1999) Melting of clusters approaching 0D. *Eur Phys J D* 9:441–444
- Liu M, Wang RY (2013) Phase change nanocomposites with tunable melting temperature and thermal energy storage density. *Nanoscale* 5:7234–7237
- Liu Z, Xu J, Chen D, Shen G (2015) Flexible electronics based on inorganic nanowires. *Chem Soc Rev* 44:161–192
- McCue SW, Wu B, Hill JM (2009) Micro/nanoparticle melting with spherical symmetry and surface tension. *IMA J Appl Math* 74:439–457
- Myers TG (2016) Mathematical modelling of phase change at the nanoscale. *Int Commun Heat Mass Trans* 76:59–62
- Wu B, McCue SW, Tillman P, Hill JM (2009a) Single phase limit for melting nanoparticles. *Appl Math Model* 33:2349–2367
- Wu B, Tillman P, Hill JM (2009b) Nanoparticle melting as a Stefan moving boundary problem. *J Nanosci Nanotechnol* 9:885–888
- Xiong S, Qi W, Cheng Y, Huang B, Wang M, Li Y (2011) Universal relation for size dependent thermodynamic properties of metallic nanoparticles. *Phys Chem Chem Phys* 13:10652–10660
- Zhang Y, Zhang HL, Wu JH, Wang XT (2011) Enhanced thermal conductivity in copper matrix composites reinforced with titanium-coated diamond particles. *Scr Mater* 65:1097–1100